

Supporting Information

**Iron(II) Complexes of 2-Mercaptopyridine as Rubredoxin Site
Analogues**

Partha Halder,^{*a} Santanu Ghorai,^a Sridhar Banerjee,^b Biswajit Mondal^b and Atanu Rana^b

a) Department of Chemistry, Scottish Church College, 1 & 3 Urquhart Square, Kolkata-700006, India. Email: icjameshalder@gmail.com

b) Department of Inorganic Chemistry, Indian Association for the Cultivation of Science, 2A & 2B Raja S. C. Mullick Road, Kolkata-700032, India.

Physical Methods and Equipments

Fourier transform infrared spectroscopy on KBr pellets was performed on a Bruker ALPHA instrument from 4000 to 400 cm⁻¹ at room temperature. Elemental analyses were performed on a Perkin Elmer 2400 series II CHN series. Electro-spray mass spectra were recorded with a Waters QTOF Micro YA263 instrument. All room temperature ¹H NMR spectra were collected on a Bruker DPX-500 spectrometer. X-band EPR measurements at 77K were performed on a JEOL JES-FA 200 instrument. Solution electronic spectra (single and time-dependent) were measured on an Agilent 8453 diode array spectrophotometer in the range of 200 to 1100 nm. Low temperature study was carried out using UNISOKU cryostat with liquid nitrogen as coolant. Electrochemical experiments were performed using CH instruments (model CHI710D Electrochemical Analyzer). GC-MS measurements were carried out with a Perkin Elmer Clarus 600 using Elite 5MS (30m x 0.25mm x 0.25μm) column with a maximum temperature of 300 °C.

X-ray crystallographic data collection and refinement and solution of the structure of 1-(OTf)₂, 1-(ClO₄)₂, and 2: X-ray single crystal data of all the complex were collected at 120 K using MoK α ($\lambda = 0.7107 \text{ \AA}$) radiation on a SMART APEX diffractometer equipped with CCD area detector. Data collection, data reduction, structure solution/refinement were carried out using the software package of APEX II.¹ The structures were solved by intrinsic methods and subsequent Fourier analyses and refined by the full-matrix least-squares method based on F^2 with all observed reflections. The non-hydrogen atoms were treated anisotropically. All the hydrogen atoms were geometrically fixed except pyridinium hydrogen which was located on a difference

Fourier map and refined. PLATON SQUEEZE² was performed to remove the distorted solvent molecules for the complex **2**.

DFT Methods

The geometry of all compounds is optimized in gradient corrected BP86 Functional in unrestricted formalism using Gaussian 03 version C03 with 6-311G(d) basis set in Fe, S atom and 6-31G(d) for other all atom.³ The fully optimized structure is confirmed by doing their frequency calculation to show no imaginary mode is present for all these compounds. The final energy calculations were performed using 6-311+G(d) basis set on all atoms in PCM model using acetonitrile as a solvent.⁴⁻⁶

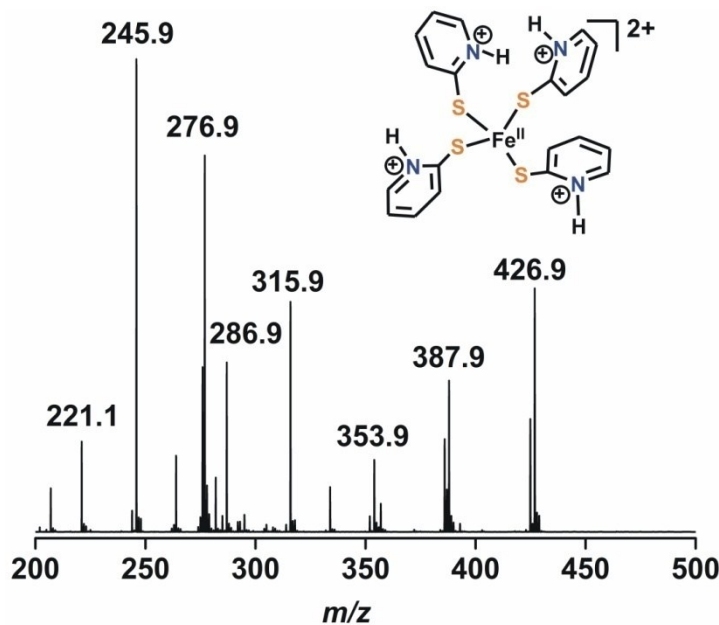


Figure S1. ESI-mass spectrum (positive ion mode, CH₃CN) of **1-(OTf)₂**.

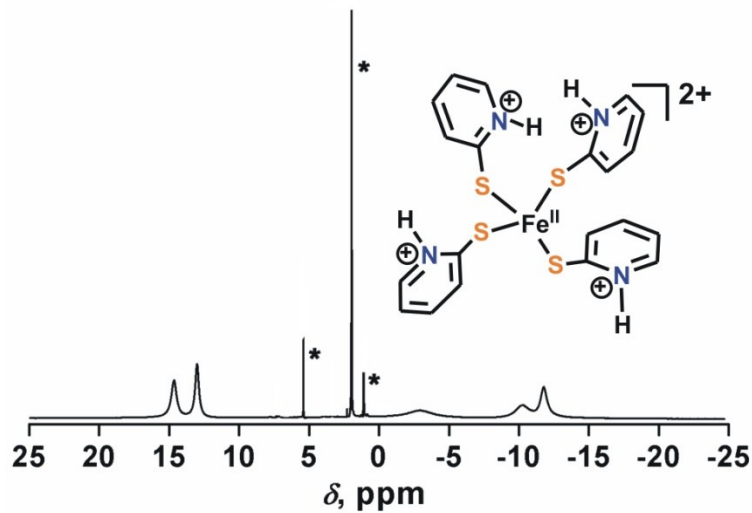


Figure S2. ^1H NMR spectrum of $\mathbf{1}-(\text{OTf})_2$ in CD_3CN at 25°C (*-marked peaks are from solvents)

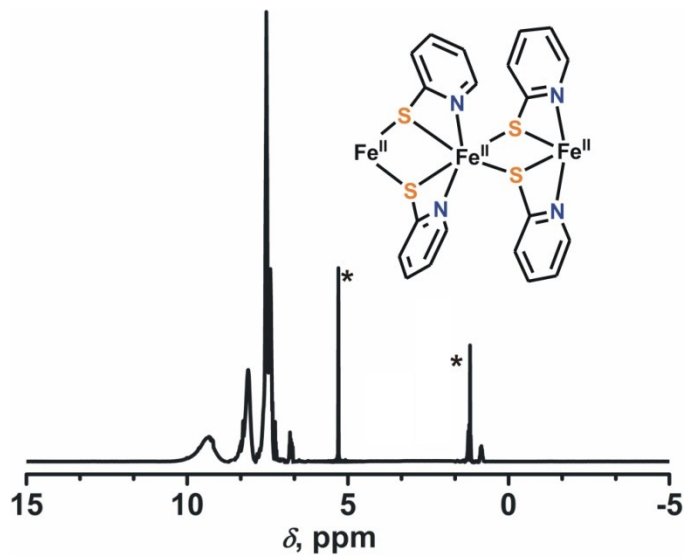


Figure S3. ^1H NMR spectrum of $\mathbf{2}$ in CDCl_3 at 25°C (*-marked peaks are from solvents)

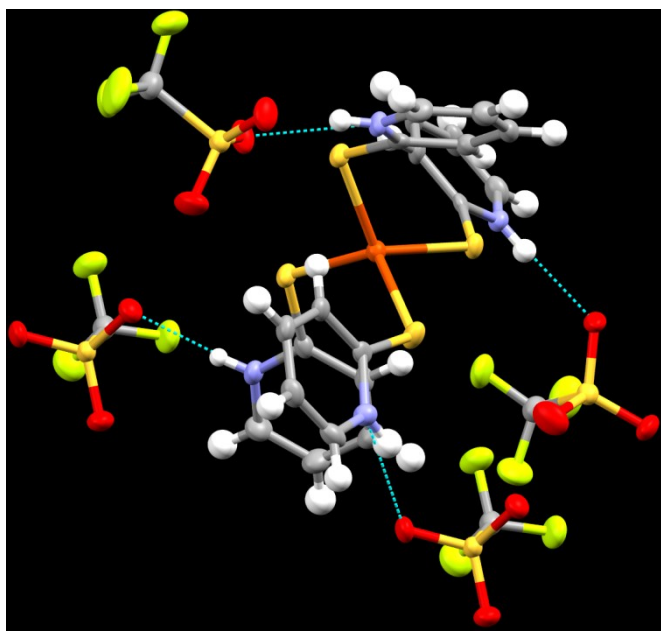


Figure S4. Crystal packing of **1**-(OTf)₂ showing hydrogen bond interaction between the protonated pyridine-2-thiolate and triflate counter anion.

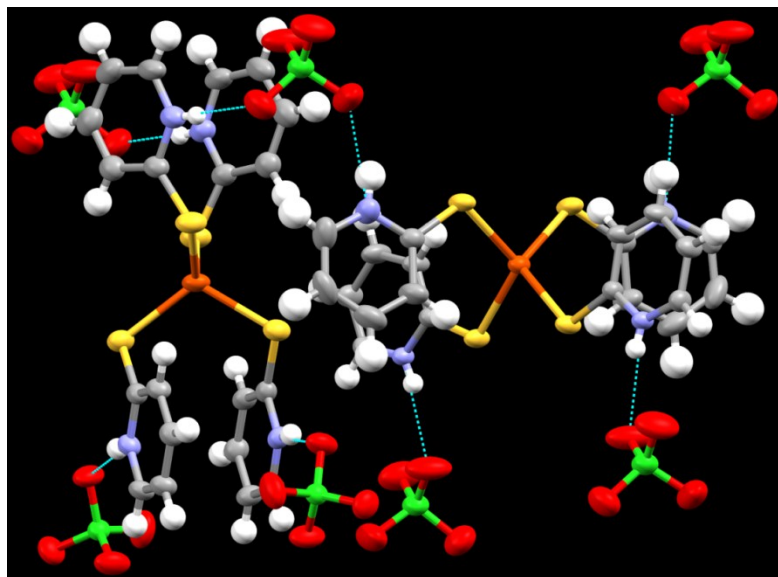


Figure S5. Crystal packing of **1**-(ClO₄)₂ showing hydrogen bond interactions between the protonated pyridine-2-thiolate and perchlorate counter anion.

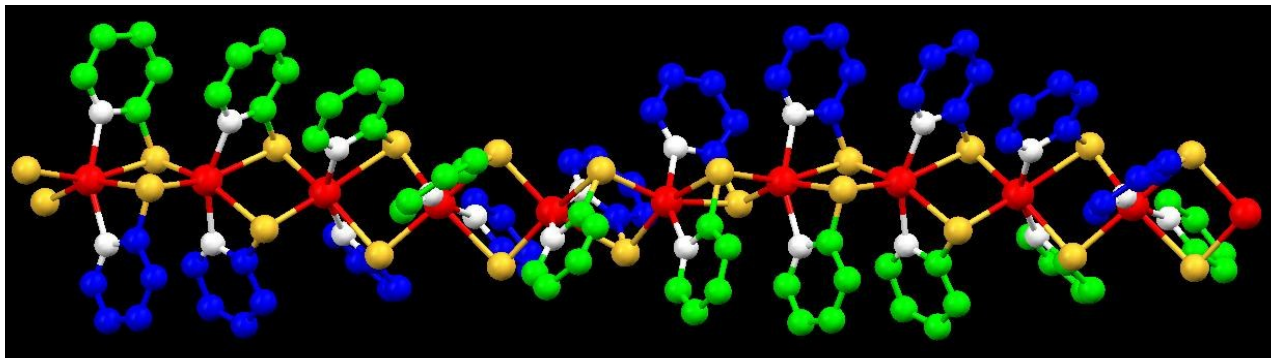


Figure S6. 1-D coordination helical coordination polymer of complex **2**.

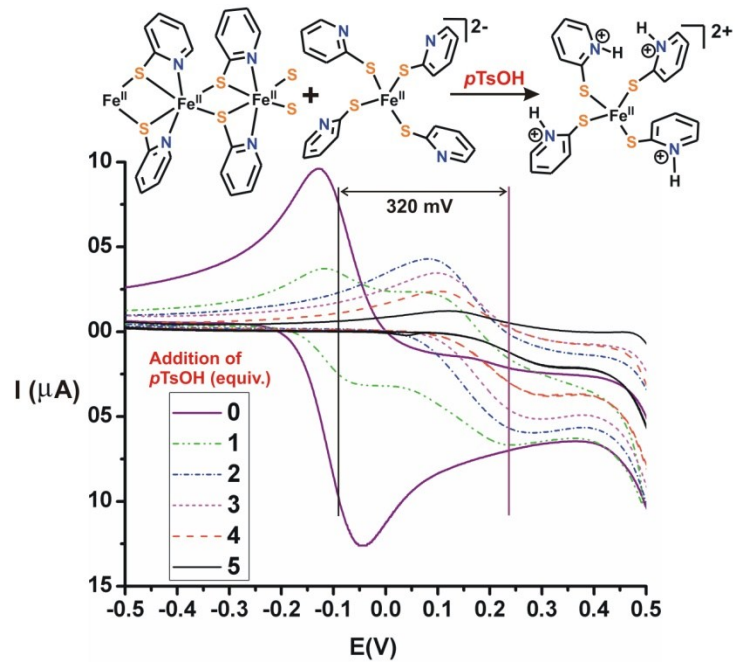


Figure S7. Overlay of CV under anaerobic condition of complex **1-(OTf)₂** (in 5 equiv. of Et_3N) upon sequential addition of $p\text{TsOH}$.

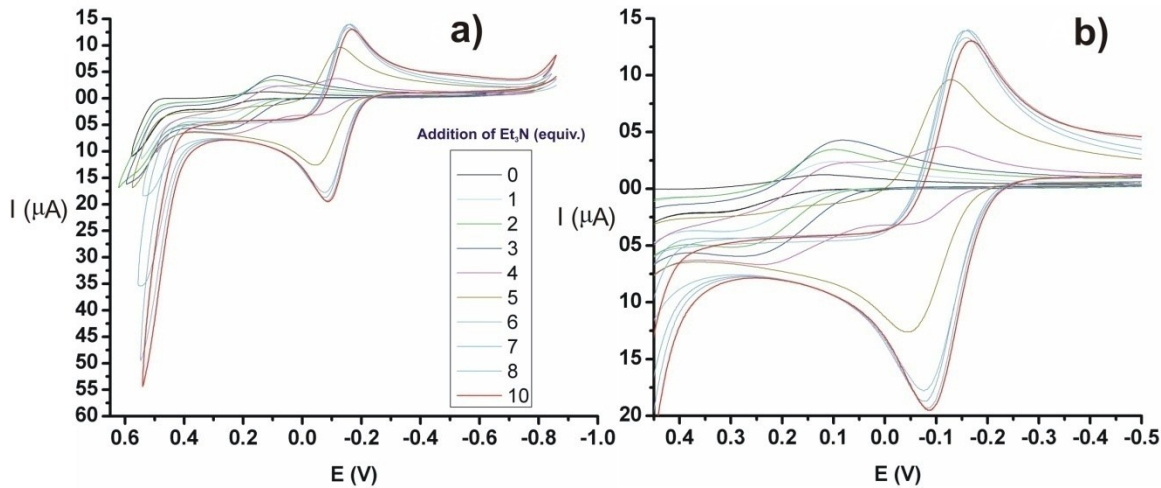


Figure S8. a) Overlay of CV of complex **1**-(OTf)₂ under anaerobic condition upon addition of Et₃N and b) its zoom portion.

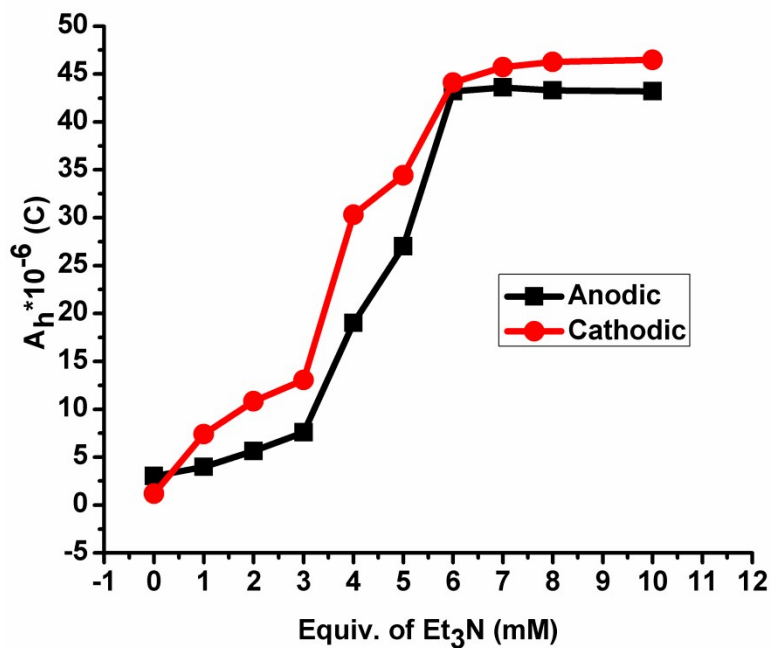


Figure S9. Area under the curve (A_h) against equivalent of Et₃N in acetonitrile solution (1 mM) of complex **1**-(OTf)₂ under inert atmosphere from Cyclic Voltammogram.

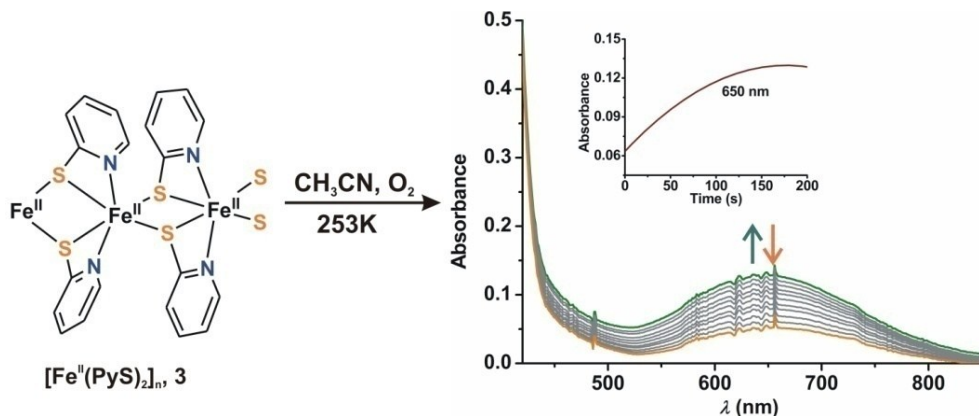


Figure S10. UV-Vis spectral change upon exposure of oxygen the acetonitrile solution (0.05 mM) of the complex **2** at -20°C.

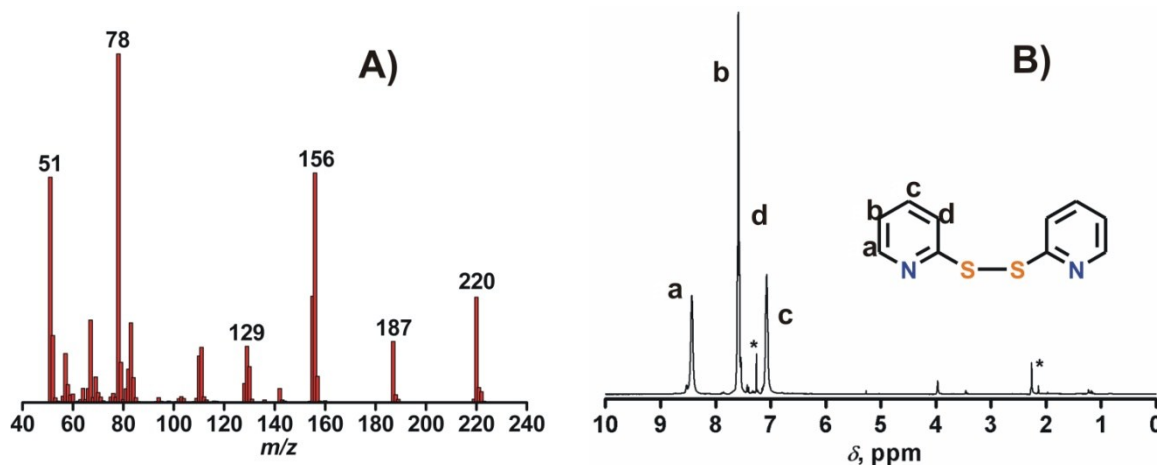


Figure S11. A) GC-MS and B) 1H NMR spectrum of the final extracted product in $CDCl_3$ at 25°C of complex **1-(OTf)₂** upon exposure of oxygen (*-marked peaks are from solvents).

Table .1 Crystallographic data for **1-(OTf)₂**, **1-(ClO₄)₂**, and **2**

Compound	1-(OTf)₂·CH₂Cl₂	1-(ClO₄)₂	2
Empirical formula	$C_{22}H_{20}F_6FeN_4O_6S_6 \cdot CH_2Cl_2$	$C_{20}H_{20}N_4Cl_2O_8S_4Fe$	$C_{20}H_{16}Fe_2N_4S_4$
Formula weight	883.56	699.39	552.31
Crystal system	Monoclinic	Monoclinic	Trigonal
Space group	$P2(1)/c$	$C2/c$	$R-3$
a , Å	10.5957(18)	15.948(5)	27.80(1)
b , Å	27.983(4)	20.583(7)	27.80(1)

c , Å	12.851(2)	18.824(6)	21.69(1)
α , deg	90.00	90.0	90.00
β , deg	112.958(4)	109.376(10)	90.00
γ , deg	90.00	90.0	120.00
Volume, Å ³	3508.5(10)	5830(3)	14522.3(14)
Z	4	8	18
$D_{\text{calcd.}}$, Mg/m ³	1.673	1.594	1.137
μ Mo-K α , mm ⁻¹	1.015	1.037	1.168
F(000)	1784	2884	5040
θ range, deg	1.46 – 24.24	1.677 – 25.789	1.26 – 24.34
Reflections collected	37048	36742	32398
Reflns unique	5565	5580	3576
$R(\text{int})$	0.0901	0.0396	0.0656
Data ($I > 2\sigma(I)$)	4499	4283	2884
Parameters	449	371	271
Goodness-of-fit on F^2	1.078	0.743	1.087
$R1$ [$I > 2\sigma(I)$]	0.0351	0.0365	0.0318
$wR2$	0.0678	0.1018	0.0771
Residuals e.Å ⁻³	0.408, -0.424	0.317, -0.350	0.194, -0.241

Table S2: Selected bond lengths (Å) and angles (°) for **1-(OTf)₂**

Fe(1)-S(1)	2.3380(9)	Fe(1)-S(2)	2.3380(9)
Fe(1)-S(3)	2.3410(10)	Fe(1)-S(4)	2.3268(10)
S(1)-C(1)	1.728(3)	S(2)-C(6)	21.736(3)
S(3)-C(11)	1.737(3)	S(4)-C(16)	1.738(3)
S(1)-Fe(1)-S(2)	117.73(3)	S(1)-Fe(1)-S(3)	93.66(3)
S(1)-Fe(1)-S(4)	112.40(3)	S(2)-Fe(1)-S(3)	116.56(3)
S(2)-Fe(1)-S(4)	100.90(3)	S(3)-Fe(1)-S(4)	116.57(4)
C(1)-S(1)-Fe(1)	109.37(11)	C(6)-S(2)-Fe(1)	103.45(11)
C(11)-S(3)-Fe(1)	114.53(11)	C(16)-S(4)-Fe(1)	108.65(11)

Table S3: Selected bond lengths (Å) and angles (°) for **1-(ClO₄)₂**

Fe(2)-S(3)	2.3272(9)	Fe(2)-S(4)	2.3284(10)
Fe(1)-S(2)	2.3506(11)	Fe(1)-S(1)	2.3556(11)
S(3)-C(15)	1.727(3)	S(4)-C(20)	1.722(3)
S(2)-C(10)	1.727(3)	S(1)-C(5)	1.728(3)
S(3)-Fe(2)-S(3')	117.73(3)	S(3)-Fe(2)-S(4')	117.43(4)
S(3)-Fe(2)-S(4)	116.55(4)	S(3')-Fe(2)-S(4)	117.43(4)

S(4)-Fe(2)-S(4')	100.57(5)	S(2)-Fe(1)-S(2')	112.25(5)
S(2)-Fe(1)-S(1')	101.05(4)	S(1)-Fe(1)-S(2)	115.8(4)
S(1)-Fe(1)-S(1')	112.97(6)	C(15)-S(3)-Fe(2)	111.34(9)

Table S4. Selected bond lengths (\AA) and angles ($^\circ$) for 2

Fe(1)-N(2)	2.108(3)	Fe(1)-N(1)	2.127(4)
Fe(1)-S(3)	2.4571(13)	Fe(1)-S(4)	2.4770(13)
Fe(1)-S(1)	2.6323 (13)	Fe(1)-S(2)	2.7285(13)
Fe(2)-N(3)	2.137(3)	Fe(2)-N(4)	2.143(4)
Fe(2)-S(2)	2.4673(12)	Fe(2)-S(1)	2.4752(13)
Fe(2)-S(3)	2.6453(12)	Fe(2)-S(4)	2.6783(13)
S(3)-C(15)	1.757(4)	S(4)-C(20)	1.734(5)
S(1)-C(5)	1.749(5)	Fe(2)-S(1)	2.4751(13)
N(2)-Fe(1)-N(1)	153.66(13)	N(2)-Fe(1)-S(3)	103.27(9)
N(1)-Fe(1)-S(3)	92.72(12)	N(2)-Fe(1)-S(4)	95.93(10)
N(1)-Fe(1)-S(4)	104.07(10)	S(3)-Fe(1)-S(4)	93.05(4)
N(2)-Fe(1)-S(1)	96.49(9)	N(1)-Fe(1)-S(1)	64.93(11)
S(3)-Fe(1)-S(1)	157.36(5)	S(4)-Fe(1)-S(1)	95.82(4)
N(2)-Fe(1)-S(2)	64.18(8)	N(1)-Fe(1)-S(2)	94.32(10)
S(3)-Fe(1)-S(2)	93.95(4)	S(4)-Fe(1)-S(2)	159.96(4)
S(1)-Fe(1)-S(2)	84.71(4)	N(3)-Fe(2)-N(4)	153.33(14)
N(3)-Fe(2)-S(2)	93.63(10)	N(4)-Fe(2)-S(2)	100.39(9)
N(3)-Fe(2)-S(1)	107.46(10)	N(4)-Fe(2)-S(1)	94.19(11)
S(2)-Fe(2)-S(1)	93.92(4)	N(3)-Fe(2)-S(3)	65.19(10)
N(4)-Fe(2)-S(3)	99.48(9)	S(2)-Fe(2)-S(3)	158.8(4)
S(1)-Fe(2)-S(3)	91.93(4)	N(3)-Fe(2)-S(4)	91.87(9)
N(1)-Fe(2)-S(4)	64.00(11)	S(2)-Fe(2)-S(4)	97.60(4)
S(1)-Fe(2)-S(4)	156.81(5)	S(3)-Fe(2)-S(4)	84.54(4)

Table S5. The bond parameters of the DFT optimized structures

Str	Fe-S1	Fe-S2	Fe-S3	Fe-S4	Fe-N3	Fe-N4	E (V)
Fe ^{II} (PySH) ₄	2.379	2.380	2.377	2.377	-	-	+0.434
Fe ^{III} (PySH) ₄	2.309	2.309	2.310	2.310	-	-	
Fe ^{II} (PySH) ₃ (PyS)	2.507	2.561	2.486	2.529	-	2.114	-0.213
Fe ^{III} (PySH) ₃ (PyS)	2.456	2.414	2.383	2.361	-	2.148	
Fe ^{II} (PySH) ₂ (PyS) ₂	2.683	2.713	2.643	2.544	2.116	2.155	-0.686
Fe ^{III} (PySH) ₂ (PyS) ₂	2.562	2.562	2.442	2.442	2.124	2.125	
Fe ^{II} (PySH)(PyS) ₃	2.516	2.355	2.343	2.408	-	-	-0.543
Fe ^{III} (PySH)(PyS) ₃	2.419	2.287	2.260	2.315	-	-	
Fe ^{II} (PyS) ₄	2.413	2.415	2.406	2.404	-	-	-0.682
Fe ^{III} (PyS) ₄	2.316	2.316	2.316	2.315	-	-	

Full Reference for Gaussian 03:

Frisch, M. J. T., G. W.; Schlegel, H. B.; Scuseria, G. E.; Robb, M. A.; Cheeseman, J. R.; Montgomery, Jr., J. A.; Vreven, T.; Kudin, K. N.; Burant, J. C.; Millam, J. M.; Iyengar, S. S.; Tomasi, J.; Barone, V.; Mennucci, B.; Cossi, M.; Scalmani, G.; Rega, N.; Petersson, G. A.; Nakatsuji, H.; Hada, M.; Ehara, M.; Toyota, K.; Fukuda, R.; Hasegawa, J.; Ishida, M.; Nakajima, T.; Honda, Y.; Kitao, O.; Nakai, H.; Klene, M.; Li, X.; Knox, J. E.; Hratchian, H. P.; Cross, J. B.; Bakken, V.; Adamo, C.; Jaramillo, J.; Gomperts, R.; Stratmann, R. E.; Yazyev, O.; Austin, A. J.; Cammi, R.; Pomelli, C.; Ochterski, J. W.; Ayala, P. Y.; Morokuma, K.; Voth, G. A.; Salvador, P.; Dannenberg, J. J.; Zakrzewski, V. G.; Dapprich, S.; Daniels, A. D.; Strain, M. C.; Farkas, O.; Malick, D. K.; Rabuck, A. D.; Raghavachari, K.; Foresman, J. B.; Ortiz, J. V.; Cui, Q.; Baboul, A. G.; Clifford, S.; Cioslowski, J.; Stefanov, B. B.; Liu, G.; Liashenko, A.; Piskorz, P.; Komaromi, I.; Martin, R. L.; Fox, D. J.; Keith, T.; Al-Laham, M. A.; Peng, C. Y.; Nanayakkara, A.; Challacombe, M.; Gill, P. M. W.; Johnson, B.; Chen, W.; Wong, M. W.; Gonzalez, C.; and Pople, J. A.; C02 ed.; Gaussian, Inc.: Wallingford CT, 2004.

References:

1. *APEX 2 v2.1–0*, Bruker AXS, Madison, WI, 2006.
2. A. L. Spek, *J. Appl. Cryst.*, 2003, **36**, 7-13.
3. A. D. Becke, *J. Chem. Phys.*, 1993, **98**, 5648-5652.
4. S. Miertus, E. Scrocco and J. Tomasi, *Chem. Phys.*, 1981, **55**, 117-129.
5. J. P. Perdew, *Phys. Rev. B*, 1986, **33**, 8822-8824.
6. R. A. Torres, T. Lovell, L. Noddleman and D. A. Case, *J. Am. Chem. Soc.*, 2003, **125**, 1923-1936.